RSC Advances

ROYAL SOCIETY OF CHEMISTRY

www.rsc.org/advances

Journal Name

ARTICLE

Controlling grain size in columnar YSZ coating formation by droplet filtering assisted PS-PVD processing

Qing-Yu Chen [a], Cheng-Xin Li [a,*], Tao Wei [b], Haibin Sun [b], Shan-Lin Zhang [a], Xiao-Tao Luo [a], Guan-Jun Yang [a], Chang-Jiu Li [a,*], Meilin Liu [b]

Received 00th January 20xx,
Accepted 00th January 20xx

DOI: 10.1039/x0xx00000x

www.rsc.org/

Grain size is important to the effect of material performance, particularly as it reduced to nanoscale size. General, ionic conductivity in solid electrolytes can be remarkable enhanced by the nanostrucutre ceramics. In this study,a shrouded plasma torch was used on plasma spray-physical vapor deposition (PS-PVD) process. Multi-stage shielding was used to realize the controlling of grain size during the deposition process. The deposition behavior of YSZ was studied. The surface and cross-sectional morphology of the coating layer were also investigated. An island structure consisting of nano particle was seen on the coating layer surface, and the particle size becomes smaller with increased shielding stage. The cross section morphology of fracture coatings showed columnar structure. In this work, the grain size of the YSZ coating layer can be successfully controlled minimum to 25 nm by PS-PVD process. The effect of YSZ grain size on the coating properties is also discussed.

Introduction

Grain size has been regarded as one of the most important factors that affects materials performance, such as the mechanical properties [1-4], the thermal conductivity[5-7], and the ionic conductivity[8,9]. Particularly, in the case of nanostructured ceramics, the presence of a large fraction of grain boundaries can lead to some new or enhanced properties[10]. One growing area of investigation is the remarkable enhancement of ionic conductivity in nanostructured solid electrolytes, known as “nanoionics”. In conventional microcrystalline solid electrolytes, the grain boundaries partially block the ionic transport, causing an extra contribution to the total resistance[11]. However, the situation is different in the case of nanostructured solid electrolytes, the total ionic conductivity increases by about one order of magnitude compared with conventional microcrystalline ceramics due to the predominance of grain-boundary conduction in the nanostructured materials, coupled with an increase in the grain-boundary ionic diffusivity with decreasing grain size[12]. Therefore, the enhanced ionic conductivities achieved by controlling grain size show a promising prospect on several applications, such as gas sensors, intermediate-temperature solid oxide fuel cells, etc. Recently, the study of materials possessing suitable grain size or morphology has become more and more important due to the difficulties of achieving optimal grain size with conventional sintering and thermal spray technology [13-18]. There is presently a strong ongoing search for modern synthesis technology for accurate and reliable grain control technology.

Plasma spray-physical vapor deposition (PS-PVD) is an emerging technology which was first proposed in 2006[19]. PS-PVD processing is operated at 50-200 Pa and can be used to deposit columnar structured yttria-stabilized-zirconia (YSZ) coatings[20-22]. The different microstructures of the coating layers, such as splats and composed of splat and columnar structure can also be prepared by PS-PVD through adjusting the process parameters such as powder feeding rate or powder properties[23-26]. During the PS-PVD deposition processing, the micro columnar structure in the YSZ coating layer can be easily formed in the form of vapor atoms or clusters. These give the possibility to control the material grain size at the nanoscale through physical vapor deposition by the PS-PVD processing. Yoshida et al. also found that the YSZ coating structure was composed of nano particles with size below 100 nm through appropriate process using hybrid plasma spray technique which is the same as the PS-PVD process[24]. In our previous research, YSZ coatings with columnar structure were successfully prepared by using a shrouded plasma torch with a 80 kW class plasma system[27]. It is also found that the plasma temperature and the electron number density has enough capability to evaporate YSZ powder[28]. However, when using low power PS-PVD system, there are still many droplets existing in the plasma jet due to the high velocity of plasma jet result to short heating time. These droplets can influence the vapor phase deposition.

a State Key Laboratory for Mechanical Behavior of Materials, School of Materials Science and Engineering, Xi'an Jiaotong University, Xi'an, Shaanxi, China
b School of Materials Science and Engineering, Center for Innovative Fuel Cell and Battery Technologies, Georgia Institute of Technology, 771 Ferst Drive, Atlanta, Georgia, USA
** State key Laboratory for Mechanical Behavior of Materials, Xi'an Jiaotong University, Xi'an Shaanxi 710049, P. R. China, E-mail: licx@mail.xjtu.edu.cn and licj@mail.xjtu.edu.cn.*

Currently there is mixed droplet and vapor phase co-deposition at the direction perpendicular to the coating. It is important to determine how to filter out the droplets. The filtering of droplets is the critical point for the control of the pure vapor phase deposition. Zhu Lin et al.[29] placed a baffle-plate in front of the substrate to partially shadow the substrate, which can filter out melted particles and obtained pure vapor phase deposition at the shadowed region. Their results proved that the coating in the unshadow region was mainly composed of the splats grain structure. The vapor phase deposition mainly contributes to a columnar-like grain structure in the shadowed region. However, the columnar structure coating layer was not attained by their experiment due to the low power and low heating ability with the largely expanded low density plasma jet in a very low pressure atmosphere.

Therefore, a controlled plasma spray system with high power is urgent for practical application to control grain size. In the present paper, a shrouded plasma torch was used to restrict the expansion of the plasma jet for enhancement of the amount of vapor phase YSZ materials. The grain size and columnar structure of the YSZ coating deposited on shadowed substrate using 80 kW class plasma systems at very low pressure is successfully controlled and investigated.

Materials and Experiments

Commercially available agglomerated 7-8 wt. % YSZ powders (Metco 6700, Sulzer-Metco, Switzerland) with mean particle size below 25 μm was used as feedstock. Well sintered YSZ wafer with dimensions of Φ18× 2 mm (diameter × thickness) was employed as a substrate for coating deposition. Prior to spraying, the substrate was polished, and then cleaned by acetone. During the spraying, the axis of the plasma jet was perpendicular to the surface of YSZ substrate and a shielding was set in front of the substrate. The schematic diagram of this setting is presented in Figure 1. Multiple substrates were placed on the same straight line to realize the multi-stage shielding during spraying operation.The plasma torch position remained fixed.

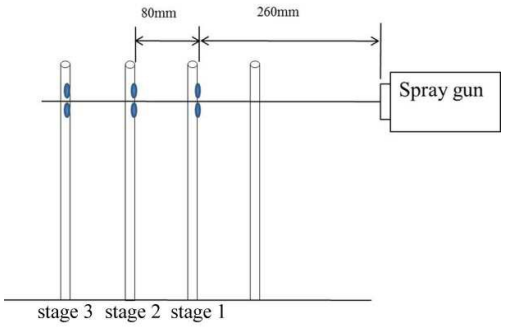

Fig.1 Schematic diagram for YSZ substrate location and the distance

A plasma spraying system (MF-P 1000 APS/VPS, GTV, Germany) equipped with an 80 kW class direct-current (DC) plasma torch was used in this study to deposit the YSZ coating. A shroud was attached in the front of the plasma torch for increasing the heating effect of plasma jet to the YSZ powder. The plasma torch was fixed on a six-axis robot which was placed in a 10 m^3 chamber. A multistage pump was used to maintain the chamber at very low pressure. The deposition conditions are summarized in Table 1. The power of the plasma torch was set from 45 kW to 78 kW. Three samples were set at intervals of 80 mm in order to constitute stage-three shielding.

The YSZ phase compositions of both powders and deposited coating were characterized by x-ray diffraction analysis (XRD, D/MAX-2400, Rigaku) using CuKα radiation. The microstructure of YSZ coating was observed by field emission scanning electron microscopy (MIRA3 LMH, TESCAN, Czech Republic). Grain size was measured by using image analysis software. Substrate temperature was tested by using thermal infrared imager (A615, FLIR, USA). The deposition time was twenty minutes.

Table.1. The deposition conditions for YSZ coatings

Parameters	Unit	Value
Power	kW	45/60/78
Chamber pressure	Pa	100
Current	A	600/680/780
Ar gas flow	slpm	40/50/70
H_2 gas flow	slpm	8/10/15
Spray distance	mm	260/340/420
Powder flow rate	g/min	3

Results

The YSZ phase compositions of powders and the deposited coating

Figure 2 shows the YSZ phase compositions of both powders and as-sprayed YSZ coating. The powder phase is mainly composed of monoclinic zirconia (m-ZrO2), but the coating layer contains the (101), (200) and (211) diffraction peaks of the tetragonal phase. The primary growth direction of the coating layers, from the maximum diffraction intensity, is that along <101> direction. The phase composition of the coating layer is mainly the metastable tetragonal zirconia (t'-ZrO2).

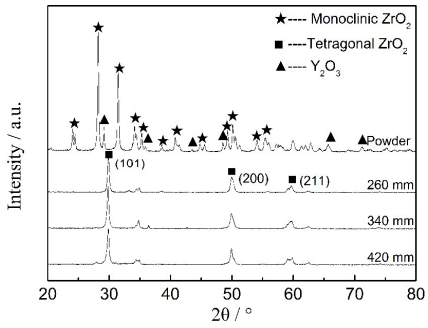

Fig.2 The XRD patterns of the YSZ powders (monoclinic) and the different distance of sprayed coating layers (tetragonal), separately.

Microstructure of the YSZ coatings

The surface morphologies of the YSZ coating layer deposited on shadowed YSZ substrate at 45 kW arc power are shown in Figure 3(a)-(f). Images (a) and (d) correspond to the sample that was placed in the 260 mm position from the spray gun. Images (b) and (e) show the microstructure of the sample that was placed another 80mm further from the spray gun. The images of the sample placed furthest from the gun are shown in(c) and (f). For an easy comparison, we can see that with the distance increment of the shielding or sample position, the unit size of island-like structures composed of YSZ decreases in size. From the high magnification images in (d), (e) and (f), all of the YSZ units of island-like structure are composed of nano particles with angular-like shape.The size of the nano angular-like particle is decreased with increasing distance from 260 mm to 420 mm corresponding to the stage of shielding increased from stage-one to stage-three.

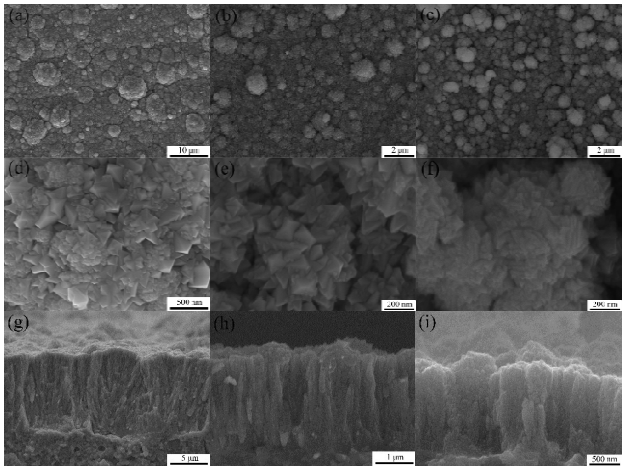

Fig.3 The surface and cross section morphology of YSZ coatings deposit on shadowed substrate at 45 kW arc power; (a), (d), and (g) 260 mm; (b), (e), and (h) 340 mm; (c), (f), and (i) 420 mm respectively.

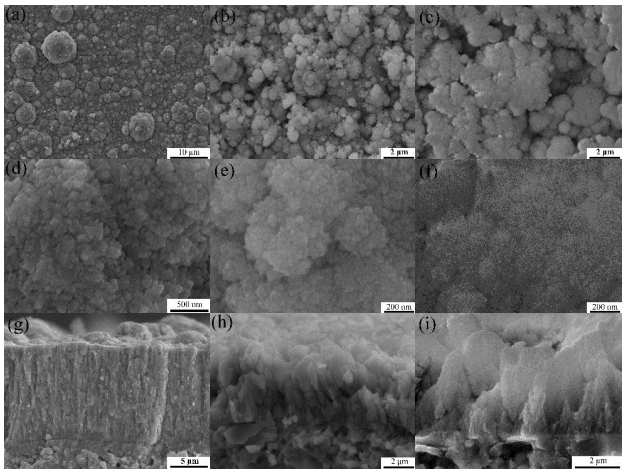

Fig.4 The surface and cross section morphology of YSZ coatings deposit on shadowed substrate at 60 kW arc power; (a), (d), and (g) 260 mm; (b), (e), and (h) 340 mm; (c), (f), and (i) 420 mm respectively.

Figure 3 (g)-(i) show the cross section morphology of the fractured YSZ coating. As shown, the thickness of the columnar structure decreased with the increased distance corresponding to increased stage of shielding. The width of the columnar structure decreased with the increased distance corresponding to increased stage of shielding, which is similar to the change rule of surface morphology as we discussed above.

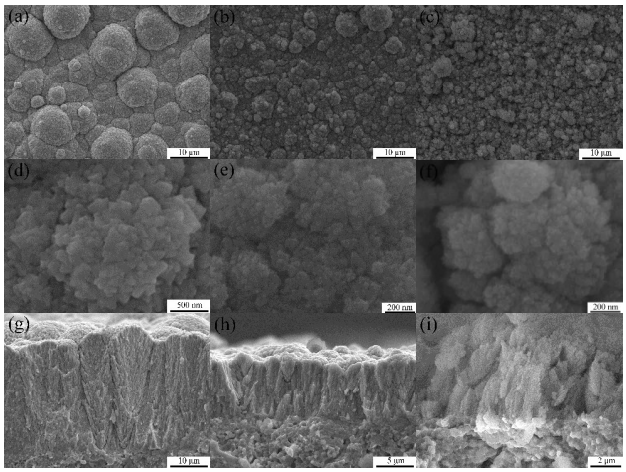

Fig.5 The surface and cross section morphology of YSZ coatings deposit on shadowed substrate at 78 kW arc power; (a), (d), and (g) 260 mm; (b), (e), and (h) 340 mm; (c), (f), and (i) 420 mm respectively.

In order to further increase the amount of YSZ vapor phase, the power of the plasma torch was increased from 45 kW to 60 kW. The morphology of the YSZ coatings, deposited with 60 kW, similarly show an island-like structure as presented in Figure. 4(a)-(f). Consistently, the particle size decreased with the increasing of shielding place distance from 260 mm to 420 mm. The high magnification images clearly show that the unit of the island-like structure is also composed of angular-like nano particles. From Figure 4(g)-(i), all of the YSZ coating cross sections show an obvious columnar structure.

When the arc power is further increased to 78 kW, in Figure 5(a)-(f), the coating surface also shows an island-like structure and the nano particle size decreased with increasing distance from 260 mm to 420 mm, and the columnar structure of the cross section is still similar to that at 60 kW and 45 kW as shown in Figure 5(g)-(i).

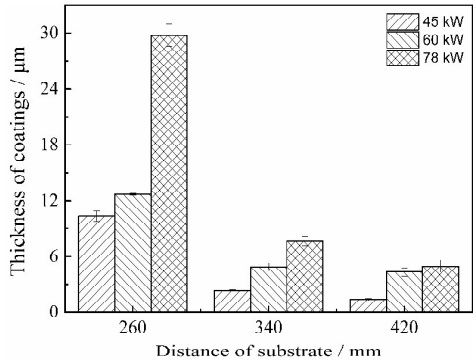

Fig.6 The thickness variation of YSZ coating layers deposited with three different distances and arc power

The thickness variation of YSZ coating layers deposited at three different distances corresponding to multi-stage shielding and with three different arc powers are shown in Figure 6. If only the arc power is changed, the deposited thickness will increase with the power increasing from 45 kW to 78 kW. For example, when the power increased from 45 kW to 78 kW, the thickness of the deposited coating significantly increased. The significant increase of arc power gives the plasma jet the ability to evaporate more powder in plasma jet. When only increasing the placing distance of the shielding from 260 mm to 420 mm, the thickness of the deposited coating also decreased gradually. One possible explanation is that the temperature of the plasma jet will reduce with the distance increase which will result in a decreas of the vapor phase concentration. The second possible reason is the distance. For example, stage-one and stage-two shielding blocks most of the vapor phase YSZ, and only a small amount can overcome the stage-three shielding to deposit on the farthest substrates.

Effect of multi-stage shielding

For YSZ coating layer deposition, multi-stage shielding installation becomes another important influencing factor for thickness control. Here, the substrate at the distance of 260 mm is taken out. The substrates at the distances of 340 mm and 420 mm become the stage one and two shielding. Using 60 kW arc power, the surface and cross section SEM images are shown in Figure 7. For 340 mm (a, c, e) and 420 mm (b, d, f) shielding distances there is an island-like surface (a, b) morphology composed of nano YSZ particles (c, d); second, the columnar structure of YSZ coating cross section is similar to our prior results. The only difference is that the coating layer becomes thicker and the diameter becomes larger when when comparing stage-one and stage-two shielding.

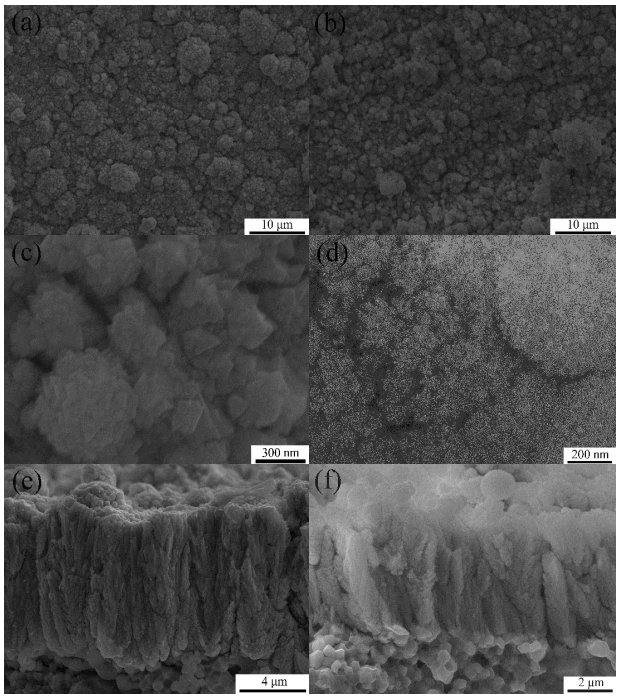

Fig.7 The surface and cross section SEM pictures of YSZ coating layer deposited at 60 kW arc power: (a), (c), (e) 340 mm as placing distance, stage-one shielding; (b), (d), (f) 420 mm as placing distance, stage-one shielding.

Furthermore, Figure 8 shows the comparison of coating thickness when deposited at different stages of shielding. Although the placing distances are the same (340 or 420 mm), the coating layer thicknesses show an apparent increase with the decrease in number of multi-stage shielding.

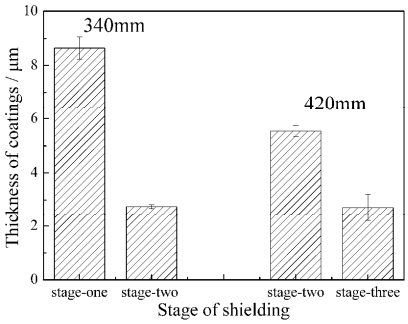

Fig.8 The comparison of coating thickness deposited at different stages of shielding.

The above testing has proven that the stages of shielding can affect the YSZ vapor phase concentration. Higher shielding stages can greatly reduce the vapor phase concentration, but only the high concentration of vapor phase can quickly grow the coating layer[30]. The coating thickness increased by two times from stage-two shielding to stage-one shielding. Distance is another influencing factor for YSZ vapor phase concentration. Even for the same stage-one shielding, the coating layer deposited at 260 mm is thicker than that at 340 mm. The coating layer thickness increased by ~50% as distance decreased from 340 mm to 260 mm. This confirmed that the shielding stages and the distance are two influencing factors on the concentration of vapor phase and coating layer thickness.

Discussion

Texture in the condition of shielding

For the condition of shielding, most of the droplet cannot deposit onto the shadowed substrate. Only the vapor phase or a few nano particles with Brownian motion are able to deposit onto the shadowed substrate. The coatings layers are mainly condensed by vapor phase YSZ solution. With the shielding processing, the primary growth direction of the coatings is oriented in the <101> direction[31], and all of the coating orientations are same for these three stages of shielding. This indicates that the orientation of the coating growth is not influenced by the shadow effect.

Deposition model of multi-stage shielding

According to the real deposition behavior of multi-stage shielding, the schematic diagram of the deposition process for multi-stage shielding is shown in Fig. 9. First the solid powder is fed into the plasma jet and heated rapidly to form the droplet and vapor phase in the plasma jet[32]. Ideally, the YSZ

droplet trajectory is in a straight line due to inertia. However, the vapor phase trajectory follows the rule of Brownian motion rather than a straight line. If there is no shielding in front of the substrate, the droplet and vapor phase will deposit directly onto the YSZ substrate. On the other hand, the shielding can greatly block the droplet transportation but the vapor phase can get around the shielding and deposit onto the back substrate. Generally, the amount of vapor phase is decreased gradually with the increased distance from 260 mm to 420 mm corresponding to the stage of shielding from stage-one to stage-three. If take away the substrate placed at 260 mm, then the substrate placed at 340 mm is became stage-one shielding. When the substrate is placed at 340 mm for stage-one shielding (no vapor consumption at the distance of 260 mm), shows in Fig. 10, the amount of YSZ vapor phase deposited on the 340 mm substrate increased. Naturally, the thickness of coating at distance of 340 mm with stage-one shielding is larger than that with stage-two shielding at the same 340 mm. Similar discipline was shows in the coatings deposited at 420 mm with stage-two and stage-three shielding.

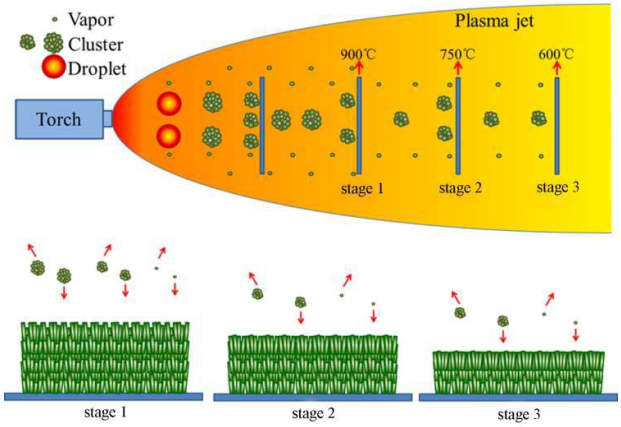

Fig.9 Schematic diagram of the YSZ coating layer deposition model with multi-stage shielding.

Influence of shielding for grain size

The amount of the deposited vapor phase YSZ and the applied arc power can greatly affect the surface morphology and the particle size of the coating layers. Figure 11 shows the average size of the island-structure and the nano-particles which compose the island-structure. For example, with a 260 mm spray distance, as in Fig. 11(a), the average size of the island-structure increased from 4.1 μm to 7.3 μm while the arc power increased from 45 kW to 78 kW. When power was increased from 45 kW to 78 kW, the size of island-structure increased from an average of 0.8μm to 4.2μm at 340 mm distance and increased from an average of 0.7μm to 3.3μm at 420 mm distance. The increased arc power can accelerate vaporization of the YSZ phase, and then the high concentration of the vapor phase can speed up the growth rate of the coating. Therefore, it tends to grow a large island-like structure. On the other one, the size of island-structure decreased with the increased distance corresponding to increased stage of shielding. This is because more vapor particles will be deposited in a short distance closer to the nozzle exit. Further, as the power is increased from 45 kW to 78 kW, in Fig. 11(b), the size of nano-particles decreases from an average of 141.6 nm to 108 nm at 260 mm distance, from an average of 75.3 nm to 45.9 nm at 340 mm distance and from an average of 48.5 nm to 25.8 nm at 420 mm distance. The above data indicates that the evaporation degree of powder increases as the arc power increases. When using low power, the degree of evaporation of YSZ powder is limited and the deposition unit is probably in the form of a cluster. With increased power, the evaporation degree of YSZ powder increased and the amount of clusters decreased. Therefore, the particle size of the island-structure decreased with increasing plasma power. It can also be seen that the particle size decreased with the distance increase from 260 mm to 420 mm corresponding to a shielding increase from stage-one to stage-three.

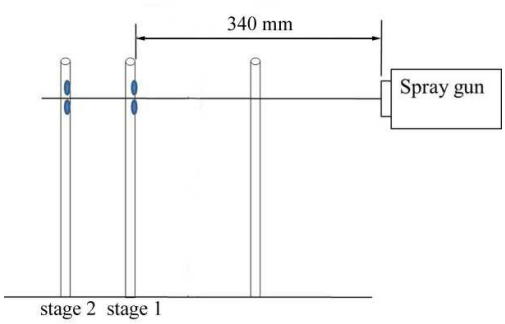

Fig.10 Schematic diagram for YSZ substrate location at defferent stage of shielding

For all the plasma power settings, from 45 kW to 78 kW, a high proportion of vapor phase YSZ will be deposited on the substrate which is close to the stage-one shielding corresponding to 260 mm distance. With highly concentrated vapor phase deposition, the island-structure will grow fast and large. The amount of vapor phase will decrease as it arrives at the second and third substrates at the two and stage-three shieldings corresponding to 340 and 420 mm distance, then the island-structures will grow slower and smaller than at the first substrate.

The size of island-structure and nano-particle at 340 mm and 420 mm deposited from different stage of shielding was shown in Fig.12. It is shown that the size of the island-structure and the nano-particles are decreased from an average of 5.1μm to 1.1μm and from an average of 81.9 nm to 48.5 nm with the stage of shielding increased from stage-one to stage-two at 340 mm distance. The size of island-structure and the nano-particle are decreased from an average of 3.9μm to 0.9μm and from an average of 34 nm to 29.6 nm, respective of the stage of shielding at stage-two and stage-three at 420 mm distance. Because a high percentage of the vapor phase will deposit on the substrate of stage-one shielding, the concentration of vapor phase will be less when deposited on the substrate of stage-two shielding or stage-three shielding.

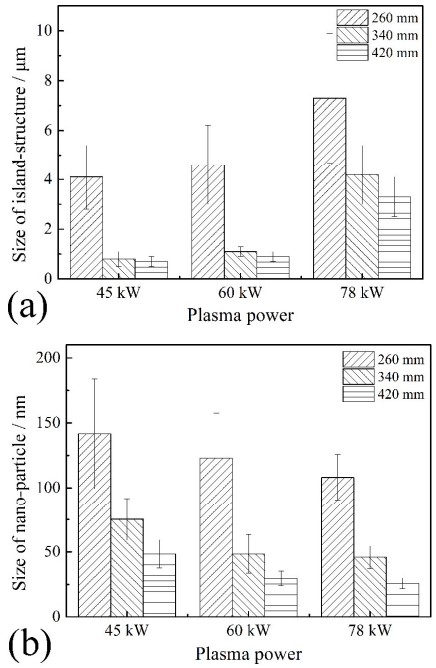

Fig.11 The size comparison of (a) the island-structure and (b) the nano-particle which composed of the island-structure

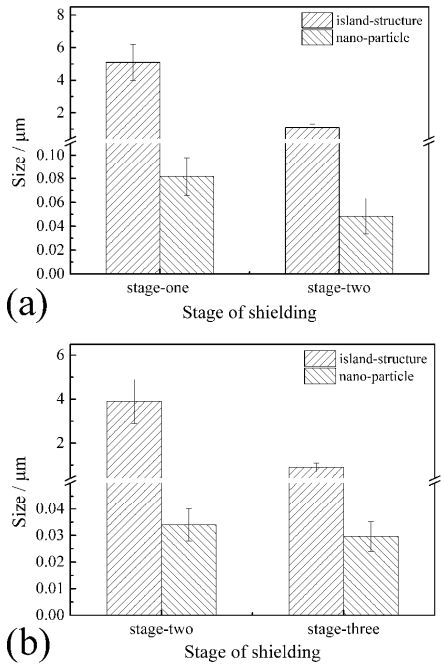

Fig.12 Particle size comparison of island-structure and nano-particle at (a) 340 mm deposited from stage-one of shielding and stage-two of shielding; (b) 420 mm deposited from stage-two of shielding and stage-three of shielding

The cluster may be formed more in the vapour phase with high concentration and on the contrary, the amount of cluster is less[33]. With increased distance, the decreased concentration of vapour phase results in less amount of cluster or smaller size of cluster and probably smaller grain size finally. On the other hand, the nano size grain may be formed during nucleation and growth[34]. When atoms and clusters arrive on the substrate, they are going to aggregate due to diffusion and nucleate as the aggregation becomes larger than the critical nucleation size. Accounting for the cluster in the vapour phase is formed from several or a dozen atoms[35]. As the diameter of of a stoichiometric 129 atoms cluster is about 1.25 nm[36]. The size of cluster formed in the vapour phase may not be larger than 25nm. Therefore, the grain size of coating is most probably formed during the nucleation. The temperature of the substrate is from 900°C to 600°C for the distance from 260mm to 420mm. The diffusion rate of the cluster and atoms is gradually decreased as distance increases from 260mm to 420mm. The grain size at 260mm distance is larger than that at 340mm and 420mm distance due to the high diffusion rate resulting in the big aggregation. In order to clear the influence of temperature of substrate on the grain size, YSZ coating was deposited at a spray distance of 260mm with one stage of shielding and the temperature of substrate was 700°C. The grain size of above coating was on average 68nm which is smaller than that deposited at 900°C temperature of substrate. Therefore, the temperature of substrate has highly effected on the nucleation and growth of vapor phase and then decided the grain size of coating. The temperature is about 15 °C to 8 °C deviation on the same substrate location from 260 mm to 420 mm if the plasma power is increased or decreased during the testing. The size deviation of nano grains is about 30 nm to 6 nm corresponds to the temperature deviation. The velocity of agglomeration and nucleation may be increased or decreased corresponds to the temperature increased or decreased. Then, the grain size deviation can be controlled in a small zone through controlling the substrate temperature.

Control of grain size on coating layer

The size of island-structure is increased with increasing power and decreased with the increased stage of shielding. Therefore, the grain size can be controlled through adjusting the arc power or the stage of shielding. So, it is possible to acquire controllable grain size, and which is important for controlling material properties. Properties such as the thermal shock resistance of materials can be influenced by the effect of grain size. Nanostructured thermal barrier coatings exhibit relatively longer lifetime than the conventional coatings at thermal cyclic testing[37-40]. Therefore, the grain size controlling of PS-PVD YSZ coating fabricated by conventional <80 kW plasma torch through droplet filtering is able to improve the performance of thermal barrier coatings. The microstructure such as grain size has highly effected on the YSZ electrolyte ionic conductivity. Ishihara et al. found that the nano-size effects positively work for increasing the oxide ionic conductivity; for example, the ionic conductivity of YSZ electrolyte increased from 107 to 209 ms/cm at 900 °C as the grain size decreased from 2.15μm to 295nm[41,42].

In order to more accurately control the electrolyte grain size, several methods were proposed such as conventional sintering (CS)[16-18, 43-47], two-step sintering (TSS)[17, 18, 46, 48], microwave sintering (MS)[16-18, 47, 49, 50], spark-plasma sintering (SPS)[18, 50-53] etc. The PS-PVD also was use to fabricate coating with fine grain size controlling[21, 23, 54-56]. The distribution of grain size

acquired through different methods was shown in Fig. 13. The grain size can be controlled as small as 90nm with conventional sintering process. With MS or SPS, the grain size can be furtherly decreased to 50nm. Even for PS-PVD with large power, the grain size was able to be decreased to 120nm. In this experiment, the grain size was decreased further to 25nm. Our testing illustrates that it is possible to manufacture nano-sized polycrystalline coatings through the droplet filtering method in the PS-PVD processing. Other method such as HIPIMS[57], DC magnetron sputtering (DMS)[58], and CVD processes[59] were also used for the controlling of grain size to nanoscales. However, the deposition rate of these method is so slow to deposit coating with thickness about 5 to10 micron. For this experiment. YSZ coating can reached about 2.7 to 30 micron at deposition time of 20 minutes which is a potential faster deposition method for electrolyte.

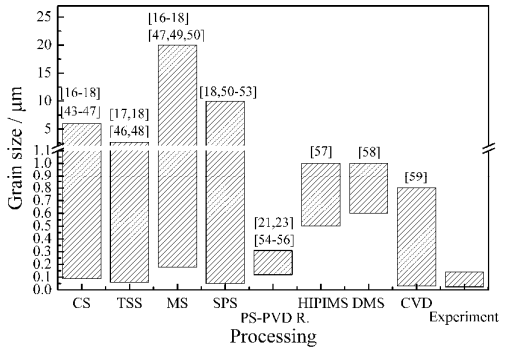

Fig.13 The distribution of grain size acquired through different method

Kosacki et al. have studied the film thickness effects on the ionic conductivity of YSZ electrolyte[60,61]. They found that the film with 29 nm thickness showed about one order of magnitude enhancement in the ionic conductivity below 650 ^{o}C than that of the film with 60 nm thickness. Sillassen et al. have found that the ionic transport along the dislocation lines in the semi-coherent interface is much faster than that in bulk and then, resulted in higher ionic conductivity at low temperature[62]. The fuel cell with 60 nm thickness polycrystalline YSZ thin film showed 270 mW cm^{-2} at 350 ^{o}C in the maximum power density[63]. It is confirmed that the ionic conductivity of YSZ electrolyte can be significant increase as the grain size decreased to < 60 nm due to the substantially increased grain boundary surface areas. As the nano grain size decreased to < 30 nm, the grain boundary surface areas may be a larger increased which expect to largely enhance the ionic conductivity of YSZ electrolyte.

The YSZ electrolyte deposited by PS-PVD with large power possibly has an effect of ionic conductivity. The smaller nano-sized coating deposited in our experiment has a potential application for large enhancement of ionic conductivity of YSZ electrolyte. General, the ionic conductivity of the coating at the direction perpendicular to the coating surface can propose to improve for the columnar structure composed of columnar structured grain.

Conclusions

The columnar-structured YSZ coatings were deposited by plasma spray-physical vapor deposition using 80 kW class plasma systems with a shrouded plasma torch at the condition of multi-stage shielding. XRD patterns show that the phase compositions of coating are composed of tetragonal zirconia which is different from the monoclinic zirconia of the powder. The surface morphologies of the coating deposited at three distances corresponding to three stages of shielding all show island-like structure, and which are composed of nano size YSZ particles. With the increased stage of shielding, the smallest size of the nano-particle can be decreased to 25nm. Both the placing distance and stage of shielding can affect the coating layer growth, and the stage of shielding seems to play a more significant role. According to the deposition behavior of the YSZ droplet, we confirmed that the coating is deposited from the vapor phase and that the grain size can be well controlled by different spray parameter adjustments.

Acknowledgements

This research work was sponsored by National Basic Research Program of China (2012CB625100) and National Natural Science Foundation of China (51342003).

References

1 C.J. Lin, Y.Y. Wang, and H. Li, J. Vac. Sci. Technol. A, 2004, 22, 2000-2004.
2 C.H. Lin, Y.Z. Tsai, and J.G. Duh, Thin Solid Films, 2010, 518, 7312-7315.
3 D.H. Jeong, F. Gonzalez, G. Palumbo, K.T. Aust and U. Erb, Scripta Mater., 2001, 44, 493-499.
4 E. Tocha, H. Schonherr, G.J. Vancso, and N. Siebelt, J. Am. Ceram. Soc., 2005, 88, 2498-2503.
5 B. Zhou, Q.S. Wang, Y.B. Liu, and Z. Ma, Mater. Prot., 2006, 39, 1-3.
6 G. Soyez, J.A. Eastman, L.J. Thompson, G.R. Bai, P.M. Baldo, A.W. McCormick, R.J. DiMelfi, A.A. Elmustafa, M.F. Tambwe, and D.S. Stone, Appl. Phys. Lett., 2000, 77, 1155-1157.
7 P.G. Klemens and M. Gell, Mat. Sci. Eng. A, 1998, 245, 143-149.
8 B.X. Wang and Z.J. Lin, Int. J. Hydrogen Energ., 2014, 39, 14334-14341.
9 R.K. Lenka, T. Mahata, A.K. Tyagi and P.K. Sinha, Solid State Ion., 2010, 181, 262–267.
10 M. G. Bellino, D. G. Lamas and N. E. Walsöe de Reca, Adv. Mater., 2006, 18, 3005-3009.
11 H. L. Tuller, Solid State Ion., 2000, 131, 143-157.
12 M. G. Bellino, D. G. Lamas and N. E. Walsöe de Reca, Adv. Funct. Mater., 2006, 16, 107-113.
13 J. Wu, H. B. Guo, L. Zhou, L. Wang, and S.K. Gong, J. Therm. Spray Techn., 2010, 19, 1186-1194.
14 Y. Tan, J. P. Longtin, S. Sampath, and H. Wang, J. Am. Ceram. Soc., 2009, 92, 710-716.
15 S.A. Tsipas and I.O. Golosnoy, J. Eur. Ceram. Soc., 2011, 31, 2923-2929.
16 X.X. Pian, B.B. Fan, H. Chen, B. Zhao, X. Zhang and R. Zhang, Ceram. Int., 2014, 40, 10483-10488.
17 M. Mazaheri, A.M. Zahedi and M.M. Hejazi, Mat. Sci. Eng. A, 2008, 492, 261-267.

18 K. Rajeswari, M.B. Suresh, U.S. Hareesh, Y.S. Rao, D. Das and R. Johnson, Ceram. Int., 2011, 37, 3557-3564.
19 T. Yoshida, Pure Appl. Chem., 2006, 78, 1093-1107.
20 A. Hospach, G. Mauer, R. Varen, and D. Stover, J. Therm. Spray Techn., 2011, 116, 116-120.
21 A. Hospach, G. Mauer, R. Vaßen and D. Stover, J. Therm. Spray Techn., 2012, 21, 435-440.
22 M. Goral, S. Kotowski, A. Nowotnik, M. Pytel, M. Drajewicz and J. Sieniawski, Surf. Coat. Tech., 2013, 237, 51-55.
23 G. Mauer, A. Hospach, and R. Vaßen, Surf. Coat. Tech., 2013, 220, 219-224.
24 H.J. Huang, K. Eguchi, M. Kambara and T. Yoshida, J. Therm. Spray Techn., 2006, 15, 83-91.
25 H.J. Huang, K. Eguchi and T. Yoshida, J. Therm. Spray Techn., 2006, 15, 72-82.
26 N. Spinhirne, D. Hirschfeld, A. Hall, and J. McCloskey, Thermal Spray 2009: Proceedings of the International Thermal Spray Conference, 2009, 750-755.
27 Q.Y. Chen, C.J. Li, C.X. Li, G.J. Yang and J.Z. Zhao, Mater. Manuf. Process, DOI:10.1080/10426914.2015.1019100.
28 Q.Y. Chen, X.Z. Peng, G.J. Yang, C.X. Li, and C.J. Li, J. Therm. Spray Techn., 2015, 24, 1038-1045
29 L. Zhu, N. N. Zhang, R. Bolot, M. P. Planche, H. L. Liao, and C. Coddet, Appl. Phys. A, 2011, 105, 991-996.
30 B.K. Jang and H. Matsubara, Scripta Mater., 2005, 52, 553-558.
31 H.S. Liu, S. Chen and P. Shen, J. Mater. Sci., 1993, 28, 3991-3996.
32 H.B. Xiong and L.L. Zheng, J. Mater. Sci. Technol., 2003, 19, 49-52.
33 Y. Ishida, T. Takahashi, H. Okumura, K. Arai and S. Yoshida, Jpn. J. Appl. Phys., 2004, 43, 5140-5144.
34 G.H. Wang, Cluster physics, Shanghai Scientific & Technical Publishers, Shanghai, Shanghai, China, 2003.
35 D.M. Mattox, Handbook of physical vapour deposition (PVD) processing, Noyes Publications, New Jersey, USA, 1998.
36 R. Grena, O. Mason, L. Portal, F. Remondiere, A. Berghout, J. Jouin, and P. Thomas, J. Phys. Chem. C, 2015, 119, 15618-15626.
37 Q. Zhang, C.J. Li, Y. Li, S.L. Zhang, X.R. Wang, G.J. Yang, and C.X. Li, J. Therm. Spray Techn., 2008, 17, 838-845.
38 M. Pourbafrani, R.S. Razavi, S.R. Bakhshi, M.R. Loghman-Estarki and H. Jamali, Surf. Eng., 2015, 31, 64-73.
39 X.D. Cheng, J. Min, X.M. Meng, H.Y. Xiang and P. Zhang, J. Aeronaut. Mater., 2012,32, 23-28.
40 Z.H. Han, H.J. Wang, S.K. Zhou and B.S. Xu, Key Eng. Mater., 2007, 336-338, 2624-2627.
41 Z.R. Hesabi, M. Mazaheri and T. Ebadzadeh, J. of Alloy Compd., 2010, 494, 362-365.
42 T. Ishihara, J.W. Yan and H. Matsumoto, Solid State Ion., 2006, 177, 1733-1736.
43 J. Obare, J. Wang and H. Conrad, Scripta Mater., 2013, 68, 111-113.
44 J. Obare, W.D. Griffin and H. Conrad, J. Mater. Sci., 2012, 47, 5141-5147.
45 B. Stawarczyk, A. Emslander, M. Roos, B. Sener, F. Noack and C. Keul, Dent. Mater. J., 2014, 33, 591-598.
46 J. Binner, K. Annapoorani, A. Paul, I. Santacruz and B. Vaidhyanathan, J. Eur. Ceram. Soc., 2008, 28, 973-977.
47 A. Borrell, M.D. Salvador, E. Rayon and F.L. Penaranda-Foix, Ceram. Int., 2012, 38, 39-43.
48 J. Tartaj and P. Tartaj, J. Am. Ceram. Soc., 2009, 92, S103-S106.
49 M.J. Kim, J.S. Ahn, J.H. Kim, H.Y. Kim and W.C. Kim, J. Adv. Prosthodont., 2013, 5, 161-166.
50 U. Anselmi-Tamburini, J.E. Garay, Z.A. Munir, A. Tacca, F. Maglia and G. Spinolo, J. Mater. Res., 2004, 19, 3255-3262.
51 G. Bernard-Granger, N. Monchalin, C. Guizard, Mater. Lett., 2008, 62, 4555-4558.
52 K. Rajeswari, M.B. Suresh, D. Chakravarty, D. Das and R. Johnson, Int. J. Hydrogen Energ., 2012, 37, 511-517.
53 X.J. Chen, K.A. Khor, S.H. Chan and L.G. Yu, Mat. Sci. Eng. A, 2003, 341, 43-48.
54 K.V. Niessen and M. Gindrat. J. Eng. Gas Turb. Power, 2011, 133, 061301-1-7.
55 A. Shinozawa, K. Eguchi, M. Kambara, and T. Yoshida, J. Therm. Spray Techn., 2010, 19, 190-197.
56 H. Huang, K. Eguchi, and T. Yoshida, Sci. Technol. Adv. Mat., 2003, 4, 617-622.
57 C.Y. Ma, P. Briois, J. Bohlmark, F. Lapostolle and A. Billard, Ionics, 2008, 14, 471-476.
58 P.K. Srivastava, T. Quach, Y.Y. Duan, R. Donelson, S.P. Jiang, F.T. Ciacchi, and S.P.S. Badwal, Solid State Ion., 1997, 99, 311-319.
59 Z. Xu, S. Yarmolenko, and J. Sankar, NATO Science Series, Series II: Mathematics, Physics and Chemistry, 2005, 202, 49-57.
60 I. Kosackia, C.M. Rouleaub, P.F. Bechera, J. Bentleya, and D.H. Lowndes, Solid State Ion., 2005, 176, 1319-1326.
61 I. Kosackia, C.M. Rouleaub, P.F. Bechera, J. Bentleya, and D.H. Lowndes, Electrochem. Solid State Lett. 2004, 7, A459-A461.
62 M. Sillassen, P. Eklund, N. Pryds, E. Johnson, U. Helmersson, and J. Bottiger, Adv. Funct. Mater., 2010, 20, 2071-2076.
63 J.H. Shim, C.C. Chao, H. Huang, and F.B. Prinz, Chem. Mater., 2007, 19, 3850-3854.

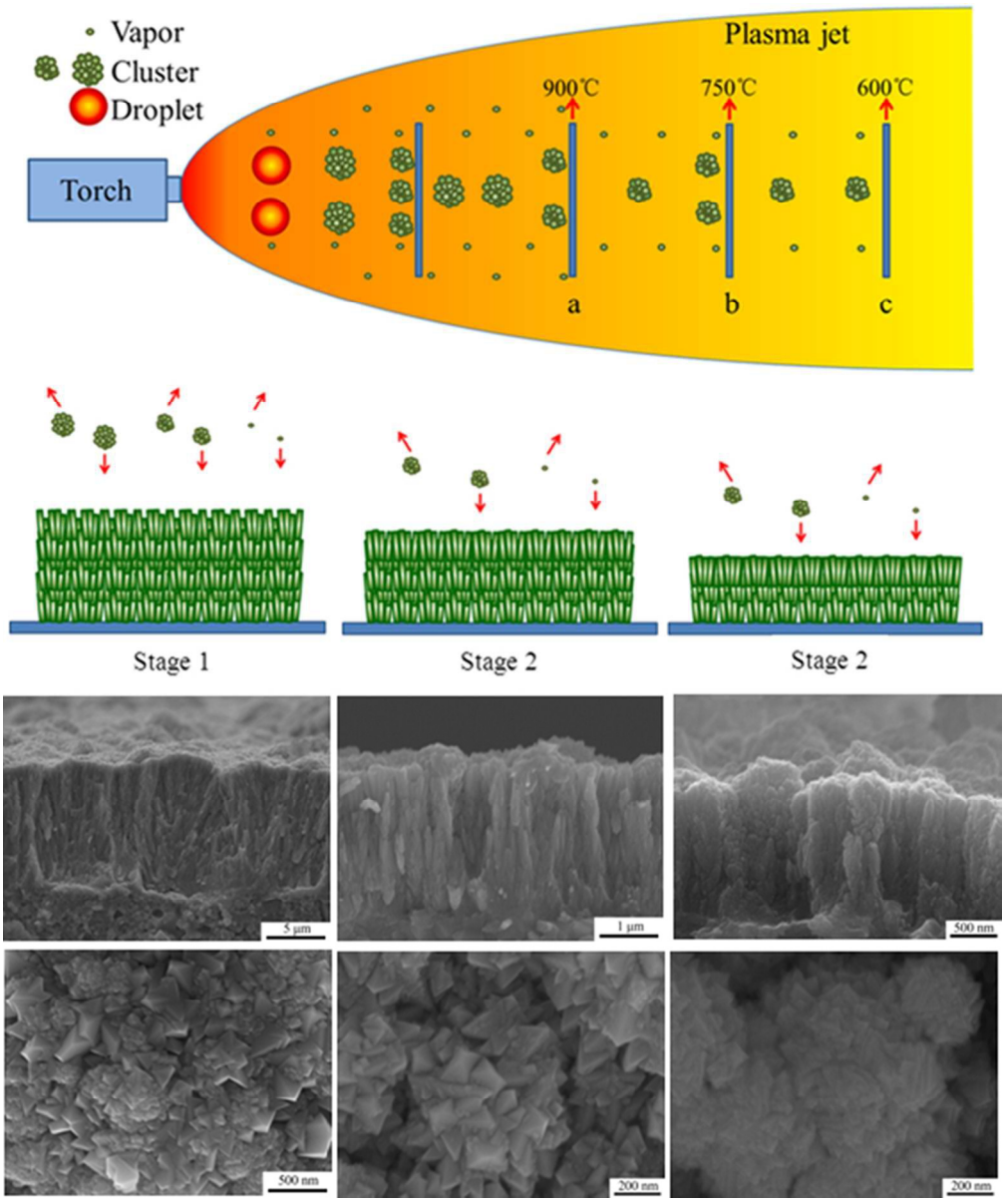

70x83mm (300 x 300 DPI)